

THEORETICAL RADII OF EXTRASOLAR GIANT PLANETS: THE CASES OF TRES-4, XO-3B, AND HAT-P-1B

XIN LIU¹, ADAM BURROWS^{1,2}, AND LAURENT IBGUI²

Accepted to ApJ, July 26, 2008

ABSTRACT

To explain their observed radii, we present theoretical radius-age trajectories for the extrasolar giant planets (EGPs) TrES-4, XO-3b, and HAT-P-1b. We factor in variations in atmospheric opacity, the presence of an inner heavy-element core, and possible heating due to orbital tidal dissipation. A small, yet non-zero, degree of core heating is needed to explain the observed radius of TrES-4, unless its atmospheric opacity is significantly larger than a value equivalent to that at $10\times$ solar metallicity with equilibrium molecular abundances. This heating rate is reasonable, and corresponds for an energy dissipation parameter (Q_p) of $\sim 10^{3.8}$ to an eccentricity of ~ 0.01 , assuming $3\times$ solar atmospheric opacity and a heavy-element core of $M_c = 30 M_\oplus$. For XO-3b, which has an observed orbital eccentricity of 0.26, we show that tidal heating needs to be taken into account to explain its observed radius. Furthermore, we reexamine the core mass needed for HAT-P-1b in light of new measurements and find that it now generally follows the correlation between stellar metallicity and core mass suggested recently. Given various core heating rates, theoretical grids and fitting formulae for a giant planet's equilibrium radius and equilibration timescale are provided for planet masses $M_p = 0.5, 1.0, \text{ and } 1.5 M_J$ with $a = 0.02\text{-}0.06$ AU, orbiting a G2V star. When the equilibration timescale is much shorter than that of tidal heating variation, the "effective age" of the planet is shortened, resulting in evolutionary trajectories more like those of younger EGPs. Motivated by the work of Jackson et al. (2008a,b), we suggest that this effect could indeed be important in better explaining some observed transit radii.

Subject headings: planetary systems — planets and satellites: general — stars: individual (HAT-P-1, GSC 02620-00648, XO-3)

1. INTRODUCTION

As of the writing of this paper, an astounding 47 transiting extrasolar giant planets (EGPs) have been discovered³. For transiting planets, the inclination/planet-mass degeneracy is resolved and the photometric dip in the stellar flux during the transit yields the planet's radius (R_p). Theory then attempts to explain the measured radii (Guillot et al. 1996; Burrows et al. 2000, 2003, 2004, 2007; Bodenheimer et al. 2001, 2003; Baraffe et al. 2003, 2004, 2008; Chabrier et al. 2004; Fortney et al. 2007; Laughlin et al. 2005). Importantly, the comparison between theory and measurement must be done for a given stellar type, orbital distance, planet mass, and age. The latter is poorly measured, but crucially important (see, e.g. §5 re HD 209458b).

Burrows et al. (2007) modeled the theoretical evolution of the radii of the 14 transiting EGPs known at the time. These authors suggest that there are two radius anomalies in the transiting EGP family, of which the smaller-radius anomaly is a result of the presence of dense cores (Mizuno 1980; Pollack et al. 1996; Hubickyj et al. 2004), whereas the larger-radius anomaly might be explained by the enhanced atmospheric opacities which slow down the heat loss of the core. They also discussed the effects on planet structure of the possible extra heat source in the interior, yet found no obvious correlation between the req-

uisite power and the intercepted stellar power. Note that none of the transiting EGPs modeled by Burrows et al. (2007) is known to have a highly eccentric orbit. However, recently several transiting EGPs with significantly non-zero eccentricities ($e \gtrsim 0.15$) have been discovered, including the EGPs XO-3b (Johns-Krull et al. 2008), HAT-P-2b (a.k.a. HD 147506b; Bakos et al. 2007a; Loeillet et al. 2008), HD 17156b (Barbieri et al. 2007; Gillon et al. 2008; Narita et al. 2008; Irwin et al. 2008), and the "hot Neptune" GJ 436b (Gillon et al. 2007; Deming et al. 2007; Demory et al. 2007).

At least for those systems with highly eccentric orbits, heating due to orbital tidal dissipation (Bodenheimer et al. 2001, 2003) should be incorporated into theoretical models for the radius-age trajectories. A preliminary exploration of this in a restricted context motivates the present paper. When the theoretical radius evolution calculations are tailored to a system's specific planet mass, age, primary stellar properties, and orbital distance (as they must), the current radii of most of the known transiting EGPs can be explained by the theoretical radius models of Burrows et al. (2007). In many instances, a higher-density core mass provides an even better fit, and extra internal heat sources are not required. However, at least three transiting EGPs seem to be exceptional in some way. The planets TrES-4 and XO-3b (for its large-radius solution based on stellar parameters from spectral synthesis modeling) are cited by their discoverers (Mandushev et al. 2007; Johns-Krull et al. 2008) as anomalously large and inconsistent with extant theoretical models. In addition, Burrows et al. (2007) found that HAT-P-1b deviated from the core-mass stellar-metallicity relationship followed by many of the transiting EGPs that they modeled (for the core-mass stellar-metallicity correlation, also see Guillot et al. 2006).

Therefore, with this paper, we focus on this small subset

¹ Department of Astrophysical Sciences, Princeton University, Peyton Hall – Ivy Lane, Princeton, NJ 08544; xinliu@astro.princeton.edu, burrows@astro.princeton.edu

² Department of Astronomy and Steward Observatory, The University of Arizona, Tucson, AZ 85721; laurent@as.arizona.edu

³ See J. Schneider's Extrasolar Planet Encyclopaedia at <http://exoplanet.eu>, the Geneva Search Programme at <http://exoplanets.eu>, and the Carnegie/California compilation at <http://exoplanets.org>

of three interesting objects to determine how their radii can indeed be explained with minimal assumptions, that nevertheless can include tidal heating. We find that tidal heating in the core, given measured (XO-3b) and possibly non-zero (TrES-4 and HAT-P-1b) eccentricities, which nevertheless are still consistent with the upper limits, can naturally explain the measured radii. For HAT-P-1b with its new age estimate, we find that a core of reasonable size can now be accommodated. Importantly, when tidal heating needs to be invoked, a canonical tidal dissipation parameter, “ Q_p ” (Goldreich & Soter 1966)⁴, with a value near 10^{4-6} , along with the measured eccentricity (or reasonable values consistent with its current bounds), suffices to explain the measurements. Hence, only simple extensions of the default evolution models that incorporate a known process with canonical parameters are required. We postulate that all measured transiting EGP radii can be explained by available theory when proper account is taken of the measured planet-star system parameters, reasonable core masses that follow the relationship between core mass and stellar metallicity (Burrows et al. 2007; Guillot et al. 2006), and tidal heating at the expected rate for non-zero, but measured, eccentricities. Exceptions to this might arise if it is determined that tidal dissipation occurs predominantly in the atmosphere, not the convective core, and/or if the eccentricity and semi-major axis history must be factored into the tidal heating history of the planet. The latter effect is intriguing and has been suggested by Jackson et al. (2008a,b).

We describe our computational techniques and model assumptions in §2. In §3, we review the measurements of these three EGP systems, identify the discrepancies between the observed planetary radii and those predicted by previous theoretical models and present new theoretical radius-age trajectories for them using tailored atmospheric boundary conditions. These new trajectories and theoretical radii include the effects of tidal heating in the convective core for measured or reasonable values of the orbital eccentricities and for a range of values for the tidal parameter, Q_p . In §4, we provide theoretical grids and fitting models for the equilibrium planetary radius and the equilibration timescale, given a certain set of planet mass, orbital distance, and tidal heating rate for a G2V primary star. Finally, in §5 we summarize our results for each system, discuss the relevant constraints obtained on their structural properties, and list caveats concerning our model assumptions.

2. COMPUTATIONAL TECHNIQUES AND MODEL ASSUMPTIONS

A detailed discussion of our computational techniques can be found in Burrows et al. (2003) and Burrows et al. (2007). Here, we present only a brief summary, along with our model assumptions. We generate realistic atmospheres customized for the three EGPs, their time-averaged orbital separations, and primary stars. The adopted atmospheric boundary conditions incorporate irradiation using the observed stellar luminosity and spectrum, and the measured planet orbital distance. For planets with eccentric orbits, the time-averaged insolation flux is employed in constructing the atmospheric boundary conditions. The theoretical stellar spectra of Kurucz (1994) are adopted. For the given stellar spectrum and flux (inferred from the luminosity and the planet orbital distance), an S - T_{eff} - g grid is calculated for the core entropy, S , effec-

tive temperature, T_{eff} , and gravity, g , using the discontinuous finite element (DFE) variant of the spectral code TLUSTY (Hubeny & Lanz 1995). It is assumed that both the stellar spectrum and flux are constant during the evolution.

We employ the Henyey evolutionary code of Burrows et al. (1997) for the radius-age evolutionary calculations, using the function $T_{eff}(S, g)$ for the interior flux, inverted from the table of S , T_{eff} , and g , referred to above. The helium fraction Y_{He} is assumed to be 0.25. We calculate models with different atmospheric opacities, the effect of which can be conveniently mimicked by using $1\times$ solar, $3\times$ solar, and $10\times$ solar abundance atmospheres. Note that the increase in atmospheric opacity does not need to, and should not be due solely to, increased metallicity. The effects of increased atmospheric opacity and increased envelope heavy-element abundances are decoupled, so that the implied increases in the heavy-element burden of the envelope, if any, will not cancel the expansion effect of enhanced atmospheric opacity (Burrows et al. 2007). To model the presence of a heavy-element core, a compressible ball of olivine is placed in the center of the model planet, and pressure continuity between the heavy-element core and the gaseous envelope is ensured throughout the evolution. We adopt the Saumon et al. (1995) equation of state (EOS) for the H_2/He envelope and the ANEOS by Thompson & Lauson (1972) for olivine.

As noted, to model the atmospheric opacity, we use supersolar metallicities (e.g., $3\times$ solar, $10\times$ solar) to mimic the expansion effects of enhanced atmospheric opacity (Burrows et al. 2007). Possible causes for such enhanced opacities might be supersolar metallicities in the atmosphere, nonequilibrium chemistry, errors in the default opacities, and thick hazes or absorbing clouds. Note that the expansion effects of enhanced atmospheric opacity and the shrinkage effects of increased envelope metallicities conceptually decoupled in our models and that an increase of the envelope heavy-element burden, will not necessarily cancel the expansion effect due to enhanced atmospheric opacity. The effect of a central heavy-element core on the planet radius is to shrink it monotonically with core mass.

Given a non-zero orbital eccentricity, the tidal dissipation rate is calculated using the formulation summarized in the Appendix (Bodenheimer et al. 2001, 2003; Gu et al. 2004). We assume that the planet is in synchronous rotation and that all the tidal heating is in the convective core. Note that the effects of other core energy dissipation mechanisms on planet structural evolution are also implicitly addressed. As indicated in the Appendix, the tidal heating rate is proportional to $f(e)/Q_p$, where $f(e) = e^2$ when $e \ll 1$. Also, the values of Q_p for EGPs with masses $M_p \sim M_J$, although very uncertain, are estimated to be $\sim 10^4 - 10^7$ (Adams & Laughlin 2006; Gu et al. 2003; Jackson et al. 2008a,b). Therefore, we calculate typical heating rates using the combination e^2/Q_p for TrES-4 and HAT-P-1b, of which the orbital eccentricities have been estimated to be $\ll 1$, if nonzero at all. Models without external heat sources ($e^2/Q_p = 0$) are also presented.

3. OBSERVED PROPERTIES AND THEORETICAL PLANETARY RADII

Table 1 displays the relevant observed quantities and the corresponding references for the EGPs TrES-4, XO-3b, and HAT-P-1b and their parent stars. These properties include semi-major axis (a), orbital period and eccentricity (e), stellar mass (M_*), radius (R_*), effective temperature T_{eff} , metallicity ($[Fe/H]_*$), age, and planetary mass (M_p) and radius

⁴ Note that the Q_p parameter used throughout this paper corresponds to the Q'_p in Mardling (2007).

(R_p). Also shown are the stellar flux at the planet's substellar point, F_p , in units of $10^9 \text{ erg cm}^{-2} \text{ s}^{-1}$, and the ratio between the possible tidal energy dissipation rate within the planet and the insolation rate $\dot{E}_{\text{tide}}/\dot{E}_{\text{insolation}}$ in the unit of $(Q_p/10^5)^{-1}$. $Q_p^{-1} \equiv \frac{1}{2\pi E_0} \oint (-\frac{dE}{dt}) dt$ is the specific dissipation function of the planet, where E_0 is the maximum energy stored in the tidal distortion and $-\frac{dE}{dt}$ is the rate of dissipation (Goldreich & Soter 1966). The parameters for TrES-4 and HAT-P-1b are drawn from Torres et al. (2008). These authors provide a uniform analysis of transit light curves and stellar parameters based on stellar evolution models, and a critical examination of the corresponding errors. Since XO-3b has not been studied by Torres et al. (2008), we generate models using parameters reported by Johns-Krull et al. (2008) and Winn et al. (2008).

Theoretical evolutionary trajectories are presented for TrES-4, XO-3b, and HAT-P-1b under various assumptions about the atmospheric opacity, the presence of a heavy-element core and possible tidal heating. The transit radius effect (Burrows et al. 2007) is also included in the models.

3.1. TrES-4

TrES-4 is the current record-holder for the lowest EGP density (Mandushev et al. 2007; Torres et al. 2008). In the discovery work, Mandushev et al. (2007) carried out spectroscopic observations with the CfA Digital Speedometer (Latham 1992), radial velocity (RV) measurements with Keck, and transit photometry in the z band with Kepler-Cam at the F. L. Whipple Observatory (FLWO) and in the B band using NASACam on the 0.8-m telescope at the Lowell Observatory. Assuming $[\text{Fe}/\text{H}]_* = 0.0^{+0.2}_{-0.2}$ dex, Mandushev et al. derived $T_{\text{eff}} = 6100^{+150}_{-150}$ K, $M_* = 1.22^{+0.17}_{-0.17} M_\odot$, $R_* = 1.738^{+0.092}_{-0.092} R_\odot$, and an age of $4.7^{+2.0}_{-2.0}$ Gyr for the star, and $M_p = 0.84^{+0.10}_{-0.10} M_J$ and $R_p = 1.674^{+0.094}_{-0.094} R_J$ for the planet. The orbital eccentricity was assumed to be exactly zero in the fit. Mandushev et al. (2007) suggested that its observed radius is too large to be explained by the theoretical EGP models of Burrows et al. (2007), given its estimated mass, age and insolation, even when the effects of higher atmospheric opacities and the transit radius correction are considered.

The parameters of TrES-4 listed in Table 1 are from Torres et al. (2008). These authors derived these parameters using the RV measurements and transit photometry from Mandushev et al. (2007), and the stellar atmospheric properties from Sozzetti et al. (2008; in preparation). Note that their estimated planetary radius $R_p = 1.751^{+0.064}_{-0.062} R_J$ is ~ 1 - σ larger than the value of $R_p = 1.674^{+0.094}_{-0.094} R_J$ of Mandushev et al. (2007).

3.1.1. Results for TrES-4

We calculate the radius-age trajectories for TrES-4 using the parameters from Torres et al. (2008), taking into account the possible effects of enhanced atmospheric opacities, and the presence of tidal dissipation given a small, yet non-zero, orbital eccentricity. Models with the presence of a heavy-element core are also calculated. The value of $\dot{E}_{\text{tide}}/\dot{E}_{\text{insolation}}$ quoted for TrES-4 in Table 1 is calculated assuming $e = 0.01$, but using all the other parameters from Torres et al. (2008) in which a circular orbit is assumed. More and better transit observations are needed to better constrain its true orbital eccentricity.

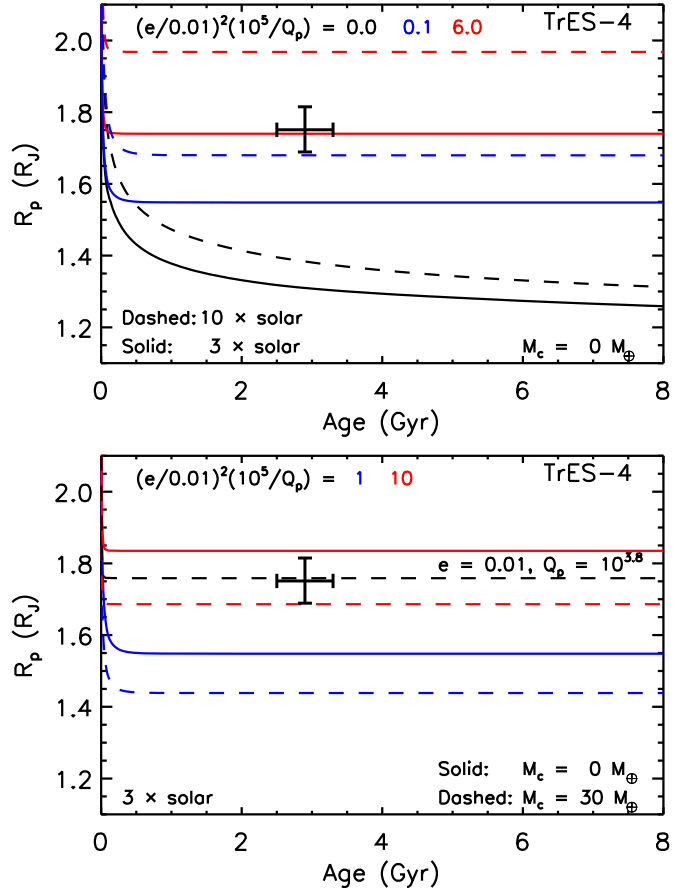


FIG. 1.— Theoretical planet radius R_p (R_J) versus age (Gyr) for TrES-4. Also shown on both panels with error bars are the observed radius and age from Torres et al. (2008). Various values are assumed concerning the atmospheric opacity, the presence of a heavy-element core, and the core heating due to tidal dissipation. Different colors correspond to different tidal heating rates, which are proportional to e^2/Q_p when $e \ll 1$ (see the Appendix for more details). *Top*: This panel demonstrates the effect of enhanced atmospheric opacity under various heating powers. Models assuming $3\times$ solar ($10\times$ solar) atmospheric opacities are plotted as solid (dashed) curves, whereas the black, blue, and red curves correspond to $(e/0.01)^2(10^5/Q_p) = 0.0, 0.1,$ and 6.0 , all without a heavy-element core ($M_c = 0$). *Bottom*: The effect of the presence of a heavy-element core is illustrated, where the dashed (solid) curves denote models with $M_c = 30$ (0) M_\oplus . If TrES-4 follows the core-mass stellar-metallicity relation found by Burrows et al. (2007), then it should contain a heavy-element core with $M_c \sim 20 - 40 M_\oplus$, given its stellar metallicity $[\text{Fe}/\text{H}]_* (+0.14^{+0.09}_{-0.09})$ dex. Assuming $3\times$ solar atmospheric opacity, the model with $Q_p = 10^{3.8}$, $e \sim 0.01$, and a heavy-element core of $M_c = 30 M_\oplus$ (black-dashed curve) explains the observed radius well.

The first panel of Fig. 1 shows the theoretical radii R_p (in units of R_J) as a function of age (in units of Gyr) for TrES-4, under various assumptions concerning the atmospheric opacity and the level of tidal dissipation, without a heavy-element core ($M_c = 0$). Models assuming $3\times$ ($10\times$) solar atmospheric opacities are shown as solid (dotted) curves. The black curves show the models without any heat sources, whereas the blue (red) curves depict those with a tidal heating rate assuming $(e/0.01)^2(10^5/Q_p) = 0.1$ (6.0). Also shown with error bars are the observed radius and age from Torres et al. (2008) (Table 1).

It can be seen from Fig. 1 that if the radius and age estimates of Torres et al. (2008) do not deviate much from their true values (within the uncertainties), our models without any heat sources produce radii which are $\sim 3\sigma$ too small. Assuming the Mandushev et al. (2007) parameters, the theoret-

ical radii are still $\sim 2\sigma$ too small. The discrepancy will become smaller for models with even higher atmospheric opacities. So it is concluded that either the atmospheric opacity of TrES-4 is unusually large (much higher than the equivalent of a $10\times$ solar metallicity, equilibrium mixture), or there are extra heat sources in the core. The required heating power is very modest; the model with $(e/0.01)^2(10^5/Q_p) = 0.1$ and $10\times$ solar atmospheric opacity produces theoretical radii consistent with the $1\text{-}\sigma$ lower bound of R_p from Torres et al. (2008).

The models shown in the first panel of Fig. 1 do not include any heavy-element cores. If TrES-4 follows the core-mass stellar-metallicity relation studied by Burrows et al. (2007), then there should be a heavy element core with $M_c \sim 20\text{--}40 M_\oplus$, given its stellar metallicity $[\text{Fe}/\text{H}]_*$ ($+0.14^{+0.09}_{-0.09}$ dex). The presence of such a heavy-element core will shrink the planetary radius, and, therefore, would require a higher tidal heating rate than do models without a core to explain the observed radius. This effect of including a heavy-element core in the models for TrES-4 is shown in the second panel of Fig. 1. Assuming $3\times$ solar atmospheric opacity, the model with $Q_p = 10^{3.8}$, $e \sim 0.01$, and a heavy-element core of $M_c = 30 M_\oplus$ (black-dashed) explains the observed radius well. Within 1σ uncertainties, the model with $Q_p = 10^{4.0}$, $e \sim 0.01$, and a heavy-element core of $M_c = 30 M_\oplus$ (red-dashed curve) can also fit the observed radius.

In summary, unless the atmospheric opacity of TrES-4 is unusually large, core heating is required to explain its observed radius. However, the required heating power is modest. A non-core model with $(e/0.01)^2(10^5/Q_p) = 0.1$ produces radii consistent with the $1\text{-}\sigma$ lower boundary of R_p from Torres et al. (2008), assuming $10\times$ solar atmospheric opacity. The required energy dissipation rates become larger for models with a heavy-element core, but are still reasonable. For instance, the model with $Q_p = 10^{3.8}$, $e \sim 0.01$, and a heavy-element core of $M_c = 30 M_\oplus$ produces the observed radius well, assuming $3\times$ solar atmospheric opacity. To better constrain models of TrES-4, definitive measurements of, or stronger limits to, its orbital eccentricity are needed.

3.2. XO-3b

XO-3b has been observed to be supermassive and on an eccentric orbit ($M_p = 13.25^{+0.64}_{-0.64} M_J$, $e = 0.260^{+0.017}_{-0.017}$; Johns-Krull et al. 2008). The discoverers obtained transit light curves with relatively small 0.3-m telescopes, spectroscopic observations using the 2.7-m Harlan J. Smith (HJS) telescope and the 11-m Hobby-Eberly Telescope (HET), and RV measurements with the HJS telescope. Based on theoretical spectral models of the HJS data, Johns-Krull et al. (2008) derive $T_{\text{eff}} = 6429^{+50}_{-50}$ K, $[\text{Fe}/\text{H}]_* = -0.177^{+0.027}_{-0.027}$ dex, and $\log g_* = 3.95^{+0.062}_{-0.062}$ for the star. Combined with the RV measurements, they arrive at $M_* = 1.41^{+0.08}_{-0.08} M_\odot$ and $R_* = 2.13^{+0.21}_{-0.21} R_\odot$ for the star, and $M_p = 13.25^{+0.64}_{-0.64} M_J$ and $R_p = 1.95^{+0.16}_{-0.16} R_J$ for the planet. These authors have commented that XO-3b is observed to be so large that in all cases analyzed by Fortney et al. (2007), their models predict a much smaller radius. However, due to the absence of a precise trigonometric parallax of XO-3, its distance is very uncertain. Assuming a smaller distance, and, hence, a reduced stellar mass and radius than obtained using the isochrone method, Johns-Krull et al. (2008) found a best fit to their transit light curves with $\log g_* = 4.19$, $M_* = 1.24 M_\odot$, and $R_* = 1.48 R_\odot$, with the correspond-

ing estimates for M_p of $12.03^{+0.46}_{-0.46} M_J$ and R_p of $1.25^{+0.15}_{-0.15} R_J$. These light-curve-based results have recently been strengthened by Winn et al. (2008) using larger aperture telescopes. These authors observed 13 transits photometrically using the 1.2-m telescope at the FLWO, along with 0.4-0.6-m telescopes. Based on these more precise transit light curves, they concluded that $\log g_* = 4.244$, $M_* = 1.213 M_\odot$, and $R_* = 1.377 R_\odot$, with the corresponding estimates for M_p of $11.79^{+0.59}_{-0.59} M_J$ and for R_p of $1.217^{+0.073}_{-0.073} R_J$. Since a trigonometric parallax measurement of XO-3 is still lacking that could distinguish these two different methods, we make models for both the spectroscopically-determined and light-curve-based parameter sets.

Both the spectroscopical results of Johns-Krull et al. (2008) and the light-curve-based results of Winn et al. (2008) are listed in Table 1. We note that the M_p and R_p values derived using the two different methods differ significantly from one another ($\sim 10\%$ in M_p and $\sim 50\%$ in R_p). Therefore, separate models and discussions for these different sets of planetary properties are in order and we calculate theoretical radii for XO-3b for both estimates of the planetary radius and mass.

3.2.1. Results for XO-3b

We include the possible heating due to orbital tidal dissipation, assuming reasonable values of Q_p . Our results for XO-3b are shown in Fig. 2, where in the first panel a planet mass of $M_p = 13.24 M_J$, derived from the spectral synthesis method of Johns-Krull et al. (2008), and an atmospheric opacity associated with $3\times$ solar metallicity are assumed, whereas in the second panel the corresponding values are $M_p = 11.79 M_J$ from the light-curve fitting results of Winn et al. (2008) and $1\times$ solar atmospheric opacity. In both cases, we assume that a massive heavy-element core is absent. For such massive planets, the effect of reasonable core masses on planetary radii is small.

As shown in the first panel of Fig. 2, the very large radius derived by Johns-Krull et al. (2008), based on spectral synthesis modeling, can be explained by energy dissipation due to tidal heating when the Q_p parameter of XO-3b is $\sim 10^{5.7}$. For the case of the light-curve-based planetary mass (second panel of Fig. 2), the inferred radius is broadly consistent to within $1\text{-}\sigma$ errors with the absence of an internal heat source, or with tidal heating with $Q_p \gtrsim 10^6$. These specific constraints on Q_p assume $3\times$ solar in the former case and $1\times$ solar atmospheric opacity in the latter. For our first model of XO-3b assuming $M_p = 13.24 M_J$ and $3\times$ solar atmospheric opacity, it would be surprising to find a planet with $R_p/R_J \lesssim 1.2$ or $\gtrsim 2.2$, since this will require Q_p to be either too large or too small. For the second model assuming $M_p = 11.79 M_J$ and $1\times$ solar atmospheric opacity, such a region would be $R_p/R_J \lesssim 1.1$ or $\gtrsim 1.6$, for the same reason. Given significant eccentricity, it is important to appropriately account for tidal heating in order to model the planet's structural evolution. We want to emphasize our adopted model assumptions that 1) the planet is in synchronous rotation and that 2) all the tidal heating is in the convective core. Even though the e^2/Q_p degeneracy is broken due to the known value of e , detailed radius evolution models could be used to constrain Q_p for EGPs, but only if it is determined that tidal dissipation occurs predominantly either in the convective core or in the atmosphere, and if the uncertainties in the core mass and atmospheric opacity are both resolved.

3.3. HAT-P-1b

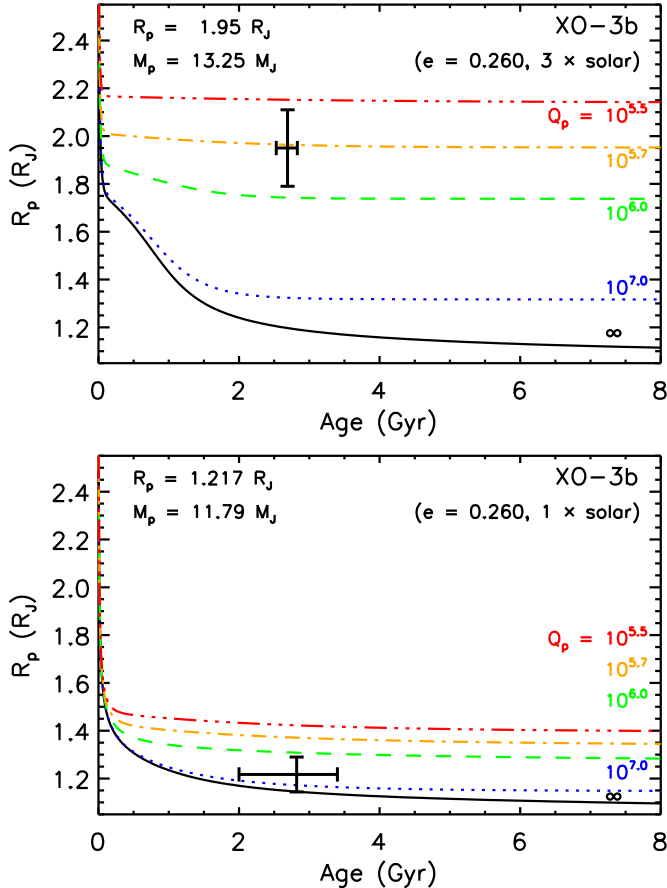


FIG. 2.— Theoretical planet radius R_p (R_J) versus age (Gyr) for XO-3b. In the first panel, a planet mass of $M_p = 13.24 M_J$ based on the spectral synthesis model of Johns-Krull et al. (2008) and $3\times$ solar atmospheric opacity are assumed, whereas in the second panel the corresponding values are $M_p = 11.79 M_J$ according to the light-curve fitting results of Winn et al. (2008) and $1\times$ solar atmospheric opacity. Also shown with error bars on both panels are the observed radii and age estimates from Johns-Krull et al. (2008) and Winn et al. (2008), based on the two different analyses. In both panels, models assuming various tidal heating rates corresponding to $Q_p = \infty$ (no heating), $10^{7.0}$, $10^{6.0}$, $10^{5.7}$, and $10^{5.5}$ are color coded. In all the models, $e = 0.260$ (Johns-Krull et al. 2008) is assumed. Note that the observed radii, based on the two different methods, differ quite a bit from one another ($\sim 50\%$). The very large radius based on spectral synthesis modeling can be fit by the model with $Q_p \sim 10^{5.7}$, whereas the much smaller one inferred from the light-curve fit can be explained by models with Q_p values down to 10^6 , within $1\text{-}\sigma$ errors. See §3.2.1 for more discussion.

Using photometry conducted by the Hungarian-made Automated Telescope Network (HATNet) project, Bakos et al. (2007b) discovered HAT-P-1b transiting one member of the stellar binary ADS 16402. These authors suggested that HAT-P-1b was too large to be explained by theoretical EGP models. Spectral synthesis modeling of the parent star ADS 16402B, based on its Keck spectra, yielded $T_{eff} = 5975^{+45}_{-45}$ K and $[\text{Fe}/\text{H}]_* = +0.13^{+0.02}_{-0.02}$ dex. Bakos et al. (2007b) also fit both stellar members in the binary to evolutionary tracks and based on the Subaru and the Keck spectra derived $M_* = 1.12^{+0.09}_{-0.09} M_\odot$ and $R_* = 1.15^{+0.10}_{-0.07} R_\odot$ for ADS 16402B and a best-fit age of 3.6 Gyr for the binary. Using the z -band transit curves from KeplerCam (Holman et al. 2006), combined with RV measurements from Subaru and Keck, these authors derive $M_p = 0.53^{+0.04}_{-0.04} M_J$ and $R_p = 1.36^{+0.11}_{-0.09} R_J$, where the errors in the planetary radius include both statistical and systematic errors in both the stellar radius and mass. Note that in the above fits,

a circular orbit ($e = 0$) was assumed. However, the χ^2 fitting of the RV data in Bakos et al. (2007b) favors a small, yet non-zero, eccentricity: $e = 0.09^{+0.02}_{-0.02}$. These authors did estimate the heating rate assuming $e = 0.09$ and suggested that if this non-zero orbital eccentricity is confirmed, the observed large R_p could be explained by tidal heating. However, note that a non-zero eccentricity is only suggestive, mainly due to the small number of RV observations (13 velocities, for which the typical S/N is about 150 per pixel). Since RV-based eccentricity estimates are positively biased due to noise (e.g., Shen & Turner 2008), it is very likely that the true e is smaller than 0.09. In fact, Johnson et al. (2008) find an upper limit on e of 0.067, with 99% confidence, by combining their new and previous RV measurements. Therefore, we assume a smaller value, $e = 0.01$, in our baseline model and see where such an assumption leads. Such a small eccentricity could result from Kozai cycles with tidal friction (e.g., Fabrycky & Tremaine 2007), though there is evidence that the spin-orbit misalignment is small (Johnson et al. 2008).

Based on more high-precision transit observations, however, Winn et al. (2007) report that HAT-P-1b is less “bloated” than originally thought. Their observations include three transits observed in z band with the 1.2-m telescope at the FLWO, three observed through the “Gunn Z” filter (Pinfield et al. 1997) using the Nickel 1-m telescope at Lick Observatory, and three observed through the Johnson I filter using the 1-m telescope at the Wise Observatory. Winn et al. (2007) derived $R_*/M_*^{1/3}$ by fitting the transit light curves, and concluded that $R_* = 1.115^{+0.043}_{-0.043} R_\odot$ and $R_p = 1.203^{+0.051}_{-0.051} R_J$. Note that in their fits the orbital eccentricity was assumed to be zero. These authors suggest that the updated radius can be explained by the structural models of Burrows et al. (2007), unless the planet has a very massive core of heavy elements. Indeed, Burrows et al. (2007) calculated radius-age trajectories for HAT-P-1b. They included different core masses and atmospheric opacities in their models, and found that in order to fit the observed radius, HAT-P-1b deviates from the stellar-metallicity versus core-mass sequence otherwise roughly followed by the transiting EGPs included in their paper (see Fig. 9 of Burrows et al. 2007). However, the stellar and planetary parameters of the HAT-P-1 system adopted by Burrows et al. (2007) are from the discovery work of Bakos et al. (2007b). The parameters of the HAT-P-1 system derived by Torres et al. (2008) are listed in Table 1. These authors compile the z -band light curves of Winn et al. (2007) and the RV data and the atmospheric parameters of Bakos et al. (2007b), but with increased uncertainties for T_{eff} , $[\text{Fe}/\text{H}]_*$, and $\log g_*$. As we show in §3.3.1, using these new parameters and the new planet radius, we now find inferred core masses that are roughly consistent with the stellar-metallicity versus core-mass relationship followed by the EGPs studied by Burrows et al. (2007).

3.3.1. Results for HAT-P-1b

Given the new measured radii and stellar age of Torres et al. (2008), we have reexamined the best-fit core masses for HAT-P-1b. The effects of the possible heating due to tidal dissipation on the planet’s structural evolution are considered, assuming a small yet non-zero eccentricity $e = 0.01$. Theoretical evolutionary trajectories of planet radius with age for HAT-P-1b are shown in Fig. 3, where the first (second) panel displays the results assuming a $3\times$ solar ($10\times$ solar) atmospheric opacity. Models with different tidal heating rates proportional to

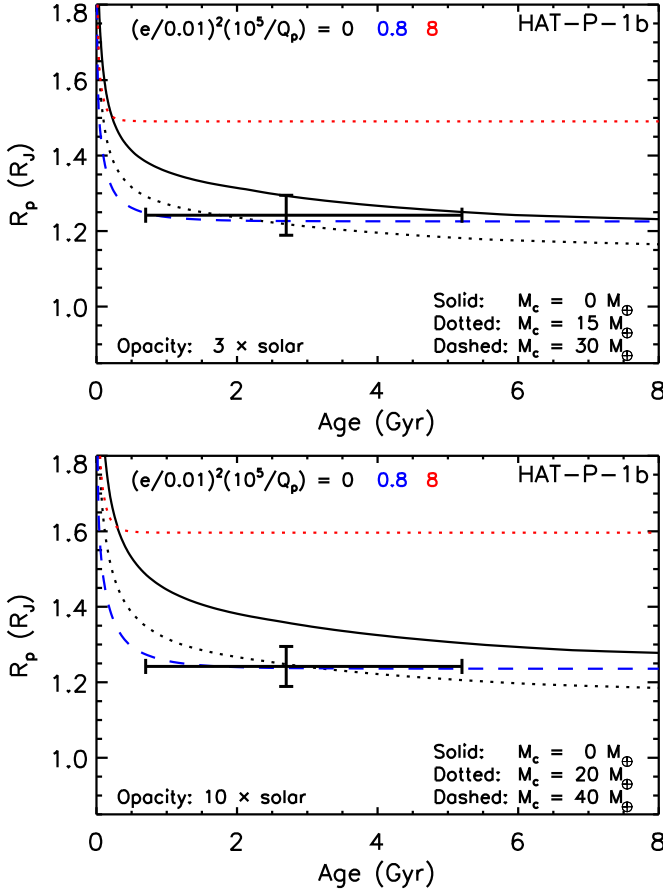


FIG. 3.— Theoretical planet radius R_p (R_J) versus age (Gyr) for HAT-P-1b. Also shown with error bars are the observational stellar age and planet radius from Torres et al. (2008), as listed in Table 1. We reexamine the best-fit core masses for HAT-P-1b, under various assumptions concerning the atmospheric opacity and the possible core heating rate due to tidal dissipation. The top (bottom) panel shows models assuming $3\times$ solar ($10\times$ solar) atmospheric opacities. In both panels, the black, blue, and red curves denote models assuming $(e/0.01)^2(10^5/Q_p) = 0, 0.8,$ and $8,$ respectively. Different line styles correspond to models with various heavy-element core masses in units of the Earth mass, M_\oplus , as labeled on the plot. If there is tidal heating assuming reasonable values of $(e/0.01)^2(10^5/Q_p) \sim 0.8$, then the core mass required to fit the observed radius is $\sim 30 M_\oplus$ ($\sim 40 M_\oplus$), assuming $3\times$ solar ($10\times$ solar) atmospheric opacity, in which case HAT-P-1b does follow the core-mass stellar-metallicity relation found by Burrows et al. (2007). See §3.3.1 for a discussion.

$(e/0.01)^2(10^5/Q_p)$ are color-coded as labeled. For both of the panels, different line styles represent “no heavy-element cores,” or the presence of a heavy-element core with a range of masses in units of Earth masses, M_\oplus . For clarity, only selected models are presented in the figure. Table 2 lists the best estimates for the core mass under various assumptions.

As demonstrated in Fig. 3 and Table 2, there are multiple solutions to explain the observed radius of HAT-P-1b. In all the cases considered, a non-zero heavy-element core mass is needed, which, without any external heat sources, is $\sim 15 M_\oplus$ ($\sim 20 M_\oplus$) assuming $3\times$ solar ($10\times$ solar) atmospheric opacity. This best-fit core mass becomes larger when there is external heating. If HAT-P-1b does follow the approximate core-mass/stellar-metallicity relation found by Burrows et al. (2007), then given its $[\text{Fe}/\text{H}]_*$ ($+0.13^{+0.08}_{-0.08}$ dex), the core mass would be $\sim 30 M_\oplus$ ($\sim 40 M_\oplus$) assuming $3\times$ solar ($10\times$ solar) atmospheric opacity. These core masses correspond to the cases with $(e/0.01)^2(10^5/Q_p) = 0.8$.

In summary, if there is tidal heating with reasonable values of Q_p , the core-mass estimates suggest that HAT-P-1b follows the correlation between stellar metallicity and core mass found by Burrows et al. (2007), or if there is no extra heating, deviates mildly from the correlation sequence. However, a larger core mass, more in keeping with the correlation found by Burrows et al. (2007), is more consistent with reasonable values of $(e/0.01)^2(10^5/Q_p)$, as long as e is non-zero and Q_p is not anomalously small.

4. EQUILIBRIUM PLANETARY RADII AND EQUILIBRATION TIMESCALES FOR VARIOUS HEATING RATES: A PARAMETER STUDY

In this section, we investigate the effects of generic core heating on the planet’s equilibrium radius, and the time to reach this equilibrium. We refer to the latter as the equilibration timescale. The heat source discussed in this section could be due to orbital tidal heating, but does not have to be. Figure 4 shows equilibrium planetary radii (R_{eq}) and equilibration timescales (τ_{eq}) with various core-heating powers, quantified by $\dot{E}_{heating}/\dot{E}_{insolation}$. Models are calculated for planets with masses $M_p = 0.5, 1.0,$ and $1.5 M_J$, with semi-major axes $a = 0.02, 0.03, 0.04, 0.05,$ and 0.06 AU, orbiting a G2V star. Equilibrium is defined as the state after which the planet radius is constant to within a part in 10^5 . We define the equilibration timescale as the time it takes the planet to evolve from $1.25 R_{eq}$ to $1.05 R_{eq}$. Note that for those rare models for which the planetary radii still change by more than $10^{-5} R_{eq}$ at the end of calculation (10 Gyr), the equilibrium state is assumed to have been reached at the final age of the evolutionary trajectory.

In Fig. 4, filled circles represent the values of R_{eq} and τ_{eq} calculated from our theoretical trajectories, whereas the curves are least-square fits to them. We adopt a fourth-order polynomial in fitting R_{eq}/R_J as a function of $\log(\dot{E}_{heating}/\dot{E}_{insolation})$, and a linear model for $\log(\tau_{eq}/\text{Gyr})$ versus $\log(\dot{E}_{heating}/\dot{E}_{insolation})$, given by:

$$\frac{R_{eq}}{R_J} = C_0 + C_1 x + C_2 x^2 + C_3 x^3 + C_4 x^4, \quad (1)$$

$$\log\left(\frac{\tau_{eq}}{\text{Gyr}}\right) = b + kx,$$

where $x \equiv \log(\dot{E}_{heating}/\dot{E}_{insolation})$. The model fits of the parameters are given in Table 3.

For an extreme close-in EGP with $M_p = 0.5 M_J$ at $a = 0.02$ AU orbiting a G2V star, the equilibrium planetary radii range from $\sim 1.3 R_J$ for little heating ($\dot{E}_{heating}/\dot{E}_{insolation} \lesssim 10^{-6}$) to $\sim 2.5 R_J$ for strong heating ($\dot{E}_{heating}/\dot{E}_{insolation} \sim 10^{-3}$). The corresponding timescales for the planet to reach these radii are ~ 3 Gyr for the former and ~ 3 Myr for the latter. At $a = 0.06$ AU, the equilibrium radii are smaller and the relevant timescales are longer – from $R_{eq} \sim 1.25 R_J$ and $\tau_{eq} \sim 2$ Gyr for $\dot{E}_{heating}/\dot{E}_{insolation} \lesssim 10^{-5}$ to $R_{eq} \sim 1.8 R_J$ and $\tau_{eq} \sim 3$ Myr for $\dot{E}_{heating}/\dot{E}_{insolation} \sim 10^{-2}$. For more massive planets, the equilibrium radii are smaller and the timescales are longer. For an EGP with $M_p = 1.5 M_J$ at $a = 0.02$ AU, the values are $R_{eq} \sim 1.8 R_J$ and $\tau_{eq} \sim 5$ Myr for $\dot{E}_{heating}/\dot{E}_{insolation} \sim 10^{-2}$. Our theoretical model grids along with the fitting curves provided in eq. (1) and the parameters listed in Table 3 can be used to calculate the equilibrium planetary radius and the typical timescale to reach it, given different combinations of planet mass, orbital distance, and the ratio of core-heating power to insola-

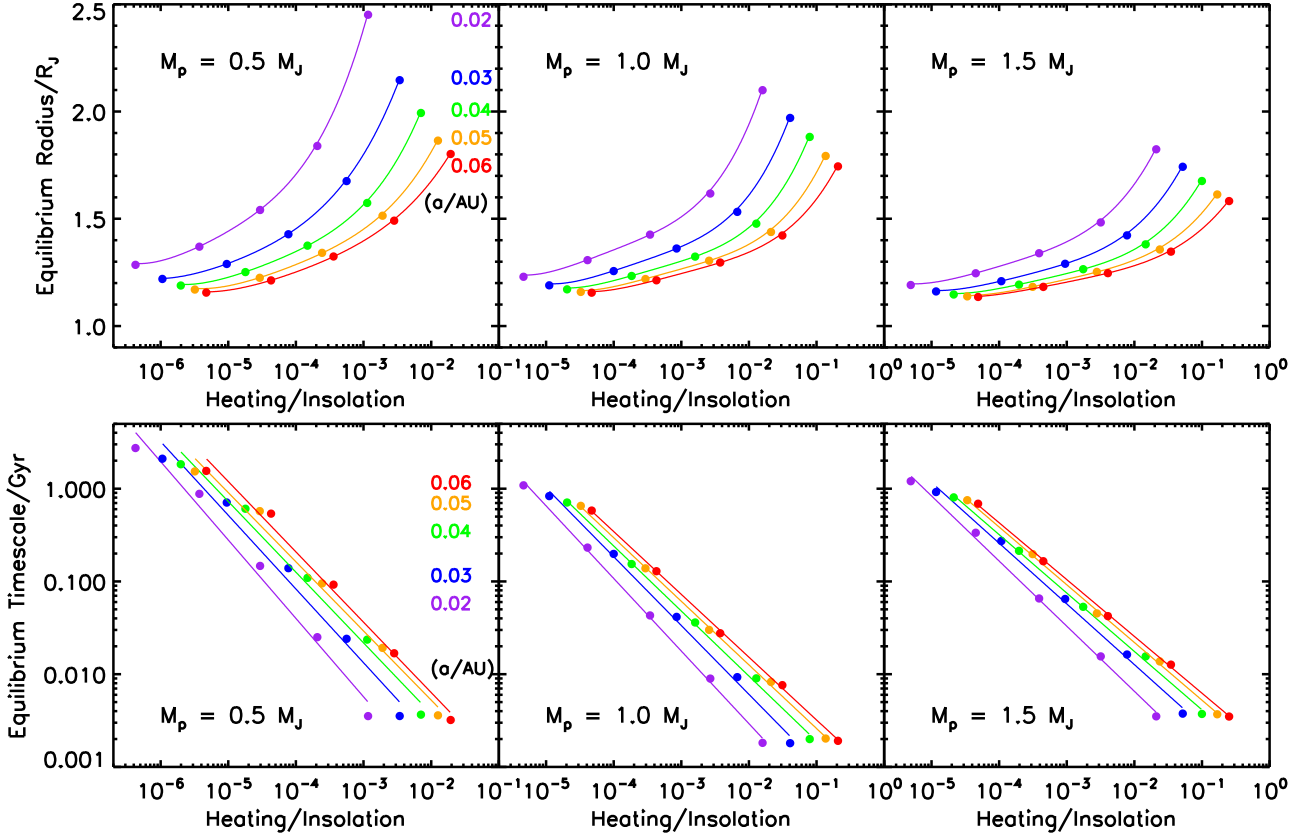


FIG. 4.— Equilibrium planetary radius R_{eq} (R_J) and equilibration timescale (Gyr) assuming various ratios between the core heating power and the insolation power. The equilibration timescale is defined as the time it takes the planet to evolve from $1.25 R_{eq}$ to $1.05 R_{eq}$. Models are calculated for planets with masses $M_p = 0.5, 1.0, \text{ and } 1.5 M_J$, and semi-major axes $a = 0.02, 0.03, 0.04, 0.05, \text{ and } 0.06$ AU, orbiting a G2V star. Filled circles represent results calculated from radius-age trajectories, whereas the curves are fits to them given by eq. (1) and the corresponding parameters in Table 3. See §4 for more information.

tion power.

5. SUMMARY AND DISCUSSION

We have calculated theoretical radius-age trajectories for three EGPs: TrES-4, XO-3b, and HAT-P-1b, under various assumptions concerning atmospheric opacity, the presence of an inner heavy-element core, and possible heating due to orbital tidal dissipation. The main model results are the following:

1. Unless the atmospheric opacity of TrES-4 is unusually large (much higher than $10\times$ solar equivalent), core heating is required to explain its observed radius ($R_p = 1.751^{+0.064}_{-0.062} R_J$; Torres et al. 2008). However, the required heating power is modest. A non-core model with $(e/0.01)^2(10^5/Q_p) = 0.1$ produces radii consistent with the $1\text{-}\sigma$ lower boundary of R_p from Torres et al. (2008), assuming $10\times$ solar atmospheric opacity. The required energy dissipation rates become larger for models with a heavy-element core. The model with $Q_p = 10^{3.8}$, $e \sim 0.01$, and a heavy-element core of $M_c = 30 M_\oplus$, reproduces the observed radius well, assuming $3\times$ solar atmospheric opacity. If TrES-4 follows the core-mass stellar-metallicity correlation found by Burrows et al. (2007), then the models with a non-zero heavy-element core mass are favored, considering its stellar metallicity $[\text{Fe}/\text{H}]_* = +0.14^{+0.09}_{-0.09}$ dex (Torres et al. 2008). Ongoing Spitzer photometry of its secondary eclipse will put more stringent constraints on e and can either confirm or rule out these possibilities.
2. For XO-3b, we have shown that orbital tidal heating is a key factor in explaining the planet radius. The very large radius ($R_p = 1.95^{+0.16}_{-0.16} R_J$) derived by Johns-Krull et al. (2008) based on spectral synthesis modeling can be explained by energy dissipation due to tidal heating. In this case, the Q_p parameter of XO-3b is near $\sim 10^{5.7}$, a not unreasonable value. On the other hand, the much smaller radius ($1.217^{+0.073}_{-0.073} R_J$) based on light-curve fit by Winn et al. (2008) is consistent with no core heating sources, or with tidal heating assuming $Q_p \gtrsim 10^6$, within $1\text{-}\sigma$ errors. These constraints on Q_p assume $3\times$ solar atmospheric opacity for the former case and $1\times$ solar for the latter, but are only weakly dependent on this.
3. We have reexamined the core mass required for HAT-P-1b using the updated data (importantly, its radius) from Torres et al. (2008), and now find it generally follows the correlation between core mass and stellar metallicity found by Burrows et al. (2007). In all the cases considered, a non-zero heavy-element core mass is needed to explain the observed radius ($R_p = 1.242^{+0.053}_{-0.053} R_J$; Torres et al. 2008). The core mass is $\sim 15 M_\oplus$ ($\sim 20 M_\oplus$) assuming $3\times$ solar ($10\times$ solar) atmospheric opacity when there is no external heating. If there is tidal heating corresponding to reasonable values of $(e/0.01)^2(10^5/Q_p) \sim 0.8$, then the core mass required to fit the observed radius is $\sim 30 M_\oplus$ ($\sim 40 M_\oplus$) assuming $3\times$ solar ($10\times$ solar) atmospheric opacity, in which case HAT-P-1b follows the core-mass stellar-metallicity re-

lation found by Burrows et al. (2007) and Guillot et al. (2006).

In addition, we have carried out a parameter study of the effects of core heating and provided theoretical grids and fitting formulae for the equilibrium planet radius and equilibration timescale, given various core heating powers for planets with masses $M_p = 0.5, 1.0,$ and $1.5 M_J$ with $a = 0.02\text{-}0.06$ AU, orbiting a G2V star. The fitting formula for the equilibrium planet radius can be used for a theoretical zeroth-order estimate, without carrying out detailed evolutionary calculations. The equilibration timescale τ_{eq} characterizes the time it takes the planet to adjust its structure in response to a given degree of core heating.

Recently Jackson et al. (2008a) considered the effect of the co-evolution of the orbital eccentricity and the semi-major axis on the tidal dissipation history. In the past, the semi-major axis had been assumed to be constant when conducting tidal evolution studies (e.g. Bodenheimer et al. 2001, 2003; Gu et al. 2004). Jackson et al. (2008b) calculate the evolutionary histories of the tidal dissipation rate for several EGPs, and find that in most cases the tidal heating rate increases as a planet moves inward and then decreases as the orbit circularizes. The relevant timescale, $\tau_{heating}$, is the time it takes the tidal heating rate to decay by a factor of e . If $\tau_{eq} \gg \tau_{heating}$, then it is valid to take a constant effective tidal heating rate in the planet radius-age trajectory calculation. If $\tau_{eq} \sim \tau_{heating}$, then in order to account for the effect of a varying tidal heating rate, different values should be used at each time step of the radius-age trajectory calculation. If $\tau_{eq} \ll \tau_{heating}$, then the planet will have enough time to reach an equilibrium radius before the tidal heating rate decays significantly. In this case, the planet’s structure evolves in a quasi-equilibrium manner. Theoretical planet radius-age trajectory models will easily be able to account for the effect of varying tidal heating rate by adopting different core heating rates at each time interval of $\tau_{heating}$ during the calculation. In effect, there is a reset of the “clock” right after the time of maximum heating – the planet becomes most extended on a timescale $\sim \tau_{eq}$ after the tidal heating rate achieves this maximum. Because of the intense heating and the quick response, the planet loses the memory of its shrinkage history before maximum heating, which is effectively a reset of its “age.”

Burrows et al. (2007) calculated theoretical radii for HD 209458b. They found that the measured radius deviated at the $\sim 1.5\text{-}\sigma$ level for the age they assumed, even when employing $10\times$ solar atmospheric opacity, no inner solid core, and no core heating. However, the updated age measure-

ment for HD 209458b by Torres et al. (2008) of $3.1^{+0.8}_{-0.7}$ Gyr is much smaller than the one adopted by Burrows et al. (2007) ($5.5^{+1.5}_{-1.5}$ Gyr), whereas the updated radius, $1.359^{+0.016}_{-0.019}$, is similar to that used by Burrows et al. (2007) ($1.32^{+0.03}_{-0.03}$). As a result, the Torres et al. (2008) radius and age measurement for HD 209458b can be fit by the $10\times$ solar-opacity model of Burrows et al. (2007) within $\sim 1\text{-}\sigma$ uncertainties, without the need of any core heating sources. Moreover, if the tidal heating rate of HD 209458b decayed from $\sim 4\times 10^{26}$ erg s^{-1} to $\sim 4\times 10^{24}$ erg s^{-1} during the past 2 Gyr (Jackson et al. 2008b), then its effective age would be 2 Gyr younger, due to the “clock reset” effect. Based on our parameter study in §4, the equilibration timescale of HD 209458b during maximum heating would have been ~ 0.05 Gyr. This is small enough compared with the decay timescale of the tidal heating rate (~ 1 Gyr from $\sim 4\times 10^{26}$ erg s^{-1} to $\sim 1.5\times 10^{26}$ erg s^{-1}) for our models to reproduce HD 209458b’s current radius. In this case, the Torres et al. (2008) radius measurement for HD 209458b, along with an “effective age” of ~ 1.1 Gyr, can explain HD 209458b’s radius within $\sim 1\text{-}\sigma$ uncertainties, even with the $1\times$ solar-opacity model of Burrows et al. (2007) and a core mass of $10\text{-}20 M_{\oplus}$, but without the need for any current core heating. The latter comports with the very small limit of ~ 0.001 on its current orbital eccentricity. A possible caveat to the tidal evolution scenarios described in Jackson et al. (2008a,b) is that they can be dramatically changed due to even a small undetected perturbing body (e.g., Mardling 2007). Sensitive searches for such companion bodies are needed to further constrain this possibility. Nevertheless, future studies should combine orbital semi-major axis, eccentricity, and planet radius evolution models in a more coupled fashion. It is not only more consistent to consider the co-evolution of a , e , and R_p , but also important to factor in the feedback of the associated tidal heating power on R_p and its radius-age trajectory (Jackson et al. 2008a,b). Such a project is in progress.

We thank Gáspár Bakos for comments on the eccentricity of HAT-P-1b, and Georgi Mandushev for insights concerning the possible eccentricity range of TrES-4. We also thank Josh Winn for a careful reading of an earlier version of the manuscript, and an anonymous referee for a careful and useful report that improves the paper. This study was supported in part by NASA grants NNG04GL22G, NNX07AG80G, and NNG05GG05G and through the NASA Astrobiology Institute under Cooperative Agreement No. CAN-02-OSS-02 issued through the Office of Space Science.

APPENDIX

EXTERNAL HEATING DUE TO TIDAL DISSIPATION

The total tidal energy dissipation rate within the planet in its rest frame assuming equilibrium tides with constant lag angle and synchronous rotation is (e.g. Goldreich & Soter 1966; Bodenheimer et al. 2001, 2003; Gu et al. 2004):

$$\begin{aligned} \dot{E}_{\text{tide}} &= \frac{GM_*\mu f(e)}{a\tau_{\text{circ}}} \\ &\approx 1.1 \times 10^{24} \text{ erg s}^{-1} \left(\frac{e}{0.01} \right)^2 \left[\frac{f(e)}{e^2} \right] \left(\frac{M_*}{M_{\odot}} \right) \left(\frac{M_p}{M_J} \right) \left(\frac{a}{0.05 \text{ AU}} \right)^{-1} \left(\frac{\tau_{\text{circ}}}{\text{Gyr}} \right)^{-1} \end{aligned} \quad (\text{A1})$$

where $\mu \equiv M_*M_p/(M_*+M_p)$ is the reduced mass, $f(e) \equiv \frac{2}{7}[h_3(e)-2h_4(e)+h_5(e)]$ is a function of orbital eccentricity with $h_3(e) = (1+3e^2+3e^4/8)(1-e^2)^{-9/2}$, $h_4(e) = (1+15e^2/2+45e^4/8+5e^6/16)(1-e^2)^{-6}$, and $h_5(e) = (1+31e^2/2+255e^4/8+185e^6/16+$

$25e^8/64)(1-e^2)^{-15/2}$ (Gu et al. 2004). Note that $f(e) \rightarrow e^2$ as $e \rightarrow 0$. τ_{circ} denotes the circularization timescale, which is

$$\tau_{\text{circ}} \approx 0.10 \text{ Gyr} \times \left(\frac{Q_p}{10^5}\right) \left(\frac{M_*}{M_\odot}\right)^{-3/2} \left(\frac{M_p}{M_J}\right) \left(\frac{R_p}{R_J}\right)^{-5} \left(\frac{a}{0.05 \text{ AU}}\right)^{13/2}. \quad (\text{A2})$$

A more informative quantity is the ratio of the tidal energy dissipation rate and the insolation rate, given by

$$\begin{aligned} \frac{\dot{E}_{\text{tide}}}{\dot{E}_{\text{insolation}}} &= \frac{GM_* \mu f(e)}{\pi F_p R_p^2 a \tau_{\text{circ}}} \\ &\approx 6.9 \times 10^{-5} \left(\frac{e}{0.01}\right)^2 \left[\frac{f(e)}{e^2}\right] \left(\frac{Q_p}{10^5}\right)^{-1} \left(\frac{M_*}{M_\odot}\right)^{5/2} \left(\frac{R_p}{R_J}\right)^3 \left(\frac{a}{0.05 \text{ AU}}\right)^{-15/2} \left(\frac{F_p}{10^9 \text{ erg cm}^{-2} \text{ s}^{-1}}\right)^{-1}. \end{aligned} \quad (\text{A3})$$

REFERENCES

- Adams, F. C. & Laughlin, G. 2006, *ApJ*, 649, 1004
- Bakos, G. Á., Kovács, G., Torres, G., Fischer, D. A., Latham, D. W., Noyes, R. W., Sasselov, D. D., Mazeh, T., Shporer, A., Butler, R. P., Stefanik, R. P., Fernández, J. M., Sozzetti, A., Pál, A., Johnson, J., Marcy, G. W., Winn, J. N., Sipőcz, B., Lázár, J., Papp, I., & Sári, P. 2007a, *ApJ*, 670, 826
- Bakos, G. Á., Noyes, R. W., Kovács, G., Latham, D. W., Sasselov, D. D., Torres, G., Fischer, D. A., Stefanik, R. P., Sato, B., Johnson, J. A., Pál, A., Marcy, G. W., Butler, R. P., Esquerdo, G. A., Stanek, K. Z., Lázár, J., Papp, I., Sári, P., & Sipőcz, B. 2007b, *ApJ*, 656, 552
- Baraffe, I., Chabrier, G., & Barman, T. 2008, *A&A*, 482, 315
- Baraffe, I., Chabrier, G., Barman, T. S., Allard, F., & Hauschildt, P. H. 2003, *A&A*, 402, 701
- Baraffe, I., Selsis, F., Chabrier, G., Barman, T. S., Allard, F., Hauschildt, P. H., & Lammer, H. 2004, *A&A*, 419, L13
- Barbieri, M., Alonso, R., Laughlin, G., Almenara, J. M., Bissinger, R., Davies, D., Gasparri, D., Guido, E., Lopresti, C., Manzini, F., & Sostero, G. 2007, *A&A*, 476, L13
- Bodenheimer, P., Laughlin, G., & Lin, D. N. C. 2003, *ApJ*, 592, 555
- Bodenheimer, P., Lin, D. N. C., & Mardling, R. A. 2001, *ApJ*, 548, 466
- Burrows, A., Guillot, T., Hubbard, W. B., Marley, M. S., Saumon, D., Lunine, J. I., & Sudarsky, D. 2000, *ApJ*, 534, L97
- Burrows, A., Hubeny, I., Budaj, J., & Hubbard, W. B. 2007, *ApJ*, 661, 502
- Burrows, A., Hubeny, I., Hubbard, W. B., Sudarsky, D., & Fortney, J. J. 2004, *ApJ*, 610, L53
- Burrows, A., Marley, M., Hubbard, W. B., Lunine, J. I., Guillot, T., Saumon, D., Freedman, R., Sudarsky, D., & Sharp, C. 1997, *ApJ*, 491, 856
- Burrows, A., Sudarsky, D., & Hubbard, W. B. 2003, *ApJ*, 594, 545
- Chabrier, G., Barman, T., Baraffe, I., Allard, F., & Hauschildt, P. H. 2004, *ApJ*, 603, L53
- Deming, D., Harrington, J., Laughlin, G., Seager, S., Navarro, S. B., Bowman, W. C., & Horning, K. 2007, *ApJ*, 667, L199
- Demory, B.-O., Gillon, M., Barman, T., Bonfils, X., Mayor, M., Mazeh, T., Queloz, D., Udry, S., Bouchy, F., Delfosse, X., Forveille, T., Mallmann, F., Pepe, F., & Perrier, C. 2007, *A&A*, 475, 1125
- Fabrycky, D. & Tremaine, S. 2007, *ApJ*, 669, 1298
- Fortney, J. J., Marley, M. S., & Barnes, J. W. 2007, *ApJ*, 659, 1661
- Gillon, M., Demory, B.-O., Barman, T., Bonfils, X., Mazeh, T., Pont, F., Udry, S., Mayor, M., & Queloz, D. 2007, *A&A*, 471, L51
- Gillon, M., Triaud, A. H. M. J., Mayor, M., Queloz, D., Udry, S., & North, P. 2008, *A&A*, 485, 871
- Goldreich, P. & Soter, S. 1966, *Icarus*, 5, 375
- Gu, P.-G., Bodenheimer, P. H., & Lin, D. N. C. 2004, *ApJ*, 608, 1076
- Gu, P.-G., Lin, D. N. C., & Bodenheimer, P. H. 2003, *ApJ*, 588, 509
- Guillot, T., Burrows, A., Hubbard, W. B., Lunine, J. I., & Saumon, D. 1996, *ApJ*, 459, L35+
- Guillot, T., Santos, N. C., Pont, F., Iro, N., Melo, C., & Ribas, I. 2006, *A&A*, 453, L21
- Holman, M. J., Winn, J. N., Latham, D. W., O'Donovan, F. T., Charbonneau, D., Bakos, G. A., Esquerdo, G. A., Hergenrother, C., Everett, M. E., & Pál, A. 2006, *ApJ*, 652, 1715
- Hubeny, I. & Lanz, T. 1995, *ApJ*, 439, 875
- Hubickyj, O., Bodenheimer, P., & Lissauer, J. J. 2004, in *Revista Mexicana de Astronomía y Astrofísica Conference Series*, Vol. 22, *Revista Mexicana de Astronomía y Astrofísica Conference Series*, ed. G. Garcia-Segura, G. Tenorio-Tagle, J. Franco, & H. W. Yorke, 83–86
- Irwin, J., Charbonneau, D., Nutzman, P., Welsh, W. F., Rajan, A., Hidas, M., Brown, T. M., Lister, T. A., Davies, D., Laughlin, G., & Langton, J. 2008, *ApJ*, 681, 636
- Jackson, B., Greenberg, R., & Barnes, R. 2008a, *ApJ*, 678, 1396
- . 2008b, *ApJ*, 681, 1631
- Johns-Krull, C. M., McCullough, P. R., Burke, C. J., Valenti, J. A., Janes, K. A., Heasley, J. N., Prato, L., Bissinger, R., Fleenor, M., Foote, C. N., Garcia-Melendo, E., Gary, B. L., Howell, P. J., Mallia, F., Masi, G., & Vanmunster, T. 2008, *ApJ*, 677, 657
- Johnson, J. A., Winn, J. N., Narita, N., Enya, K., Williams, P. K. G., Marcy, G. W., Sato, B., Ohta, Y., Taruya, A., Suto, Y., Turner, E. L., Bakos, G., Butler, R. P., Vogt, S. S., Aoki, W., Tamura, M., Yamada, T., Yoshii, Y., & Hidas, M. 2008, *ArXiv e-prints*, 806
- Kurucz, R. 1994, *Solar abundance model atmospheres for 0,1,2,4,8 km/s*. Kurucz CD-ROM No. 19. Cambridge, Mass.: Smithsonian Astrophysical Observatory, 1994., 19
- Latham, D. W. 1992, in *Astronomical Society of the Pacific Conference Series*, Vol. 32, *IAU Colloq. 135: Complementary Approaches to Double and Multiple Star Research*, ed. H. A. McAlister & W. I. Hartkopf, 110–119
- Laughlin, G., Wolf, A., Vanmunster, T., Bodenheimer, P., Fischer, D., Marcy, G., Butler, P., & Vogt, S. 2005, *ApJ*, 621, 1072
- Loillet, B., Shporer, A., Bouchy, F., Pont, F., Mazeh, T., Beuzit, J. L., Boisse, I., Bonfils, X., da Silva, R., Delfosse, X., Desort, M., Ecuivillon, A., Forveille, T., Galland, F., Gallenne, A., Hébrard, G., Lagrange, A.-M., Lovis, C., Mayor, M., Moutou, C., Pepe, F., Perrier, C., Queloz, D., Ségransan, D., Sivan, J. P., Santos, N. C., Tsodikovich, Y., Udry, S., & Vidal-Madjar, A. 2008, *A&A*, 481, 529
- Mandushev, G., O'Donovan, F. T., Charbonneau, D., Torres, G., Latham, D. W., Bakos, G. Á., Dunham, E. W., Sozzetti, A., Fernández, J. M., Esquerdo, G. A., Everett, M. E., Brown, T. M., Rabus, M., Belmonte, J. A., & Hillenbrand, L. A. 2007, *ApJ*, 667, L195
- Mardling, R. A. 2007, *MNRAS*, 382, 1768
- Mizuno, H. 1980, *Progress of Theoretical Physics*, 64, 544
- Narita, N., Sato, B., Ohshima, O., & Winn, J. N. 2008, *PASJ*, 60, L1+
- Pinfield, D. J., Hodgkin, S. T., Jameson, R. F., Cossburn, M. R., & von Hippel, T. 1997, *MNRAS*, 287, 180
- Pollack, J. B., Hubickyj, O., Bodenheimer, P., Lissauer, J. J., Podolak, M., & Greenzweig, Y. 1996, *Icarus*, 124, 62
- Saumon, D., Chabrier, G., & van Horn, H. M. 1995, *ApJS*, 99, 713
- Shen, Y. & Turner, E. L. 2008, *ArXiv e-prints*, 806
- Thompson, S. L. & Lauson, H. S. 1972, *Sandia National Laboratory Report*, SC-RR-71, 0714
- Torres, G., Winn, J. N., & Holman, M. J. 2008, *ApJ*, 677, 1324
- Winn, J. N., Holman, M. J., Bakos, G. Á., Pál, A., Asher Johnson, J., Williams, P. K. G., Shporer, A., Mazeh, T., Fernandez, J., Latham, D. W., & Gillon, M. 2007, *AJ*, 134, 1707
- Winn, J. N., Holman, M. J., Torres, G., McCullough, P., Johns-Krull, C. M., Latham, D. W., Shporer, A., Mazeh, T., Garcia-Melendo, E., Foote, C., Esquerdo, G., & Everett, M. 2008, *ArXiv e-prints*, 804

TABLE 1
OBSERVATIONAL PROPERTIES OF THE TRANSITING PLANET SYSTEMS.

System	a (AU)	Period (days)	e	M_* (M_\odot)	R_* (R_\odot)	T_{eff} (K)	[Fe/H] $_*$ (dex)	Age (Gyr)	M_p (M_J)	R_p (R_J)	F_p^a ($10^9 \text{ erg cm}^{-2} \text{ s}^{-1}$)	$\dot{E}_{\text{tide}}/\dot{E}_{\text{insolation}}^b$ [[$Q_p/10^5$] $^{-1}$]	References
XO-3	0.0476 $^{+0.0005}_{-0.0005}$	3.19154	0.260 $^{+0.017}_{-0.017}$	1.41 $^{+0.08}_{-0.08}$	2.13 $^{+0.21}_{-0.21}$	6429 $^{+50}_{-50}$	-0.177 $^{+0.027}_{-0.027}$	2.69 $^{+0.14}_{-0.16}$	13.25 $^{+0.64}_{-0.64}$	1.95 $^{+0.16}_{-0.16}$	4.20 $^{+0.84}_{-0.84}$	5.9×10^{-1}	c
.	0.0454 $^{+0.00082}_{-0.00082}$	3.19152	0.260 $^{+0.017}_{-0.017}$	1.213 $^{+0.066}_{-0.066}$	1.377 $^{+0.083}_{-0.083}$	6429 $^{+100}_{-100}$	-0.177 $^{+0.080}_{-0.080}$	2.82 $^{+0.58}_{-0.82}$	11.79 $^{+0.59}_{-0.59}$	1.217 $^{+0.073}_{-0.073}$	1.93 $^{+0.27}_{-0.27}$	3.1×10^{-1}	d
TrES-4	0.05092 $^{+0.00072}_{-0.00069}$	3.553945	~ 0.0	1.394 $^{+0.060}_{-0.056}$	1.816 $^{+0.065}_{-0.062}$	6200 $^{+75}_{-75}$	+0.14 $^{+0.09}_{-0.09}$	2.9 $^{+0.4}_{-0.4}$	0.920 $^{+0.073}_{-0.072}$	1.751 $^{+0.064}_{-0.062}$	2.31 $^{+0.21}_{-0.20}$	$2.3 \times 10^{-4} e$	f
HAT-P-1	0.0553 $^{+0.0012}_{-0.0013}$	4.46543	~ 0.0	1.133 $^{+0.075}_{-0.079}$	1.135 $^{+0.048}_{-0.048}$	5975 $^{+120}_{-120}$	+0.13 $^{+0.08}_{-0.08}$	2.7 $^{+2.5}_{-2.0}$	0.532 $^{+0.030}_{-0.030}$	1.242 $^{+0.053}_{-0.053}$	0.66 $^{+0.08}_{-0.08}$	$9.2 \times 10^{-5} e$	f

^a The stellar flux at the planet's substellar point.

^b \dot{E}_{tide} is the total tidal energy dissipation rate within the planet in its rest frame (Gu et al. 2004). $\dot{E}_{\text{insolation}} \equiv \pi R_p^2 F_p$.

^c Johns-Krull et al. (2008); Inferred from spectroscopically derived stellar parameters.

^d Winn et al. (2008); Determined from light-curve fits.

^e Assuming $e = 0.01$.

^f Torres et al. (2008); Note that they assume $e = 0$ exactly in deriving the parameters, since the radial-velocity data are consistent with a circular orbit.

TABLE 2
BEST-ESTIMATE CORE MASSES FOR HAT-P-1B UNDER
VARIOUS ASSUMPTIONS.

Atmospheric Opacity	3×solar			10×solar			
	$\left(\frac{e}{0.01}\right)^2 \left(\frac{10^5}{Q_p}\right)$	0	0.8	8	0	0.8	8
M_c/M_\oplus		15	30	60	20	40	80

NOTE. — The tidal dissipation rate is proportional to e^2/Q_p when $e \ll 1$.

TABLE 3
FITTING PARAMETERS FOR THE EQUILIBRIUM PLANETARY RADIUS AND
EQUILIBRATION TIMESCALE FOR EGPs UNDERGOING CORE HEATING.

M_p (M_J)	a (AU)	C_0^a	C_1^a	C_2^a	C_3^a	C_4^a	b^b	k^b
0.5	0.02	15.4	9.69	2.63	0.328	0.0156	-4.78	-0.845
....	0.03	7.74	4.43	1.22	0.157	0.00785	-4.26	-0.794
....	0.04	6.42	4.00	1.25	0.182	0.0101	-3.95	-0.762
....	0.05	4.61	2.66	0.866	0.135	0.00809	-3.77	-0.746
....	0.06	3.60	1.79	0.573	0.0905	0.00560	-3.71	-0.758
1.0	0.02	6.42	4.51	1.58	0.255	0.0155	-4.10	-0.783
....	0.03	4.44	3.02	1.16	0.208	0.0139	-3.70	-0.742
....	0.04	3.42	2.19	0.894	0.170	0.0122	-3.42	-0.701
....	0.05	2.72	1.54	0.669	0.137	0.0106	-3.27	-0.686
....	0.06	2.33	1.15	0.512	0.110	0.00897	-3.17	-0.677
1.5	0.02	4.20	2.54	0.888	0.145	0.00899	-3.59	-0.702
....	0.03	3.15	1.76	0.663	0.118	0.00796	-3.21	-0.654
....	0.04	2.57	1.34	0.543	0.105	0.00762	-3.01	-0.630
....	0.05	2.13	0.924	0.391	0.0808	0.00634	-2.90	-0.622
....	0.06	1.91	0.693	0.292	0.0610	0.00486	-2.82	-0.612

^a $R_{eq}/R_J = C_0 + C_1x + C_2x^2 + C_3x^3 + C_4x^4$, where $x \equiv \log(\dot{E}_{heating}/\dot{E}_{insolation})$.

^b $\log(\tau_{eq}/\text{Gyr}) = b + kx$.